Available online at www.sciencedirect.com
SCIENCE DIRECT®
Computers and Structures 83 (2005) 856–869
Computers & Structures
www.elsevier.com/locate/compstruc

# Three-dimensional boundary element assessment of a fibre/matrix interface crack under transverse loading

Adrián P. Cisilino [a,*], Jhonny E. Ortiz [b]

[a] Department of Mechanical Engineering, Welding and Fracture Division—INTEMA—CONICET, Universidad Nacional de Mar del Plata, Av. Juan B. Justo 4302, (7600) Mar del Plata, Argentina
[b] Department of Mechanical Engineering, Faculty of Engineering, Universidad Nacional de Trujillo, Trujillo, Perú

Accepted 6 September 2004

**Abstract**

The macroscopic behaviour of unidirectional fibre-reinforced-composite materials is strongly dependent on the strength of the fibre/matrix adhesion. The stress concentrations around the fibres lead to micro-crack initiation, which will grow along a ply to become a complete transverse crack. In this paper a boundary element methodology for the three-dimensional analysis of bimaterial interface cracks is presented. Fracture mechanics parameters, namely $J$-integral and stress intensity factors, are computed along the crack front using the Energy Domain Integral and the $M_1$-integral methodologies. The devised numerical tool is employed to analyse the problem of a fibre/matrix interface crack under transverse loading in order to assess the three-dimensional character of the problem, and to evaluate the representatives of the results obtained from two-dimensional models. Obtained results show the key role played by the relative elastic properties of the fibre, the matrix and the laminate on the state of mixed mode fracture.


*Keywords:* Composite materials; Interface crack; Boundary elements; Interaction integral

## 1. Introduction

Unidirectional composite materials are known to have highly anisotropic properties, with excellent stiffness and strength characteristics in the fibre direction and rather poor properties in the transverse direction. For this reason, in practice, laminates are used consisting of several stacked plies with different fibre orientations, resulting in sufficient stiffness in more than one direction. However, mechanical loading of such structures also induces loads in arbitrary directions non-coincident either with those of the fibre or the applied load. The main cause of early failure of the transverse ply is the heterogeneity of the material. It has been shown that a global strain of 1% already gives local strains of more than 5% [1]. An irregular packing of fibres, due to the inhomogeneous fibre distribution increases the effect. Due to this local stress concentration, the macroscopic transverse failure strain is, in most cases, considerably lower than the longitudinal failure strain.

In all loading directions, the macroscopic behaviour of unidirectional fibre-reinforced-composite materials is strongly influenced by the phenomena occurring at the

* Corresponding author. Tel.: +54 223 4816600x247; fax: +54 223 4810046.
*E-mail address:* cisilino@fi.mfp.edu.ar (A.P. Cisilino).

0045-7949/$ - see front matter © 2004 Published by Elsevier Ltd.
doi:10.1016/j.compstruc.2004.09.012

fibre scale. In longitudinal as well as in transverse direction, the stress transfer from the matrix to the fibres governs the mechanical behaviour of the composite, as the failure process is mainly determined by the strength of the fibre/matrix adhesion. The stress concentrations around the fibres lead to micro-crack initiation, which will grow along a ply to become a complete transverse crack. An example of this phenomenon is illustrated in Fig. 1.

During the past few decades, comprehensive analyses have been carried out and many questions regarding the mechanic of interface fracture have been answered. However, progress has been generally focused in the two-dimensional idealization of an interface crack, and limited work has been conducted on the three-dimensional aspect of interface fracture. This is in part due to the extreme complexity of such problems and the very large computational efforts required for their numerical analysis. However, given the material mismatch at the interface boundary, it is expected that the three-dimensional effects play a more significant role in a bimaterial structure than in a homogenous structure.

The attraction of the BEM can be largely attributed to the reduction in the dimensionality of the problem; for two-dimensional problems, only the line-boundary of the domain needs to be discretized into elements, and for three-dimensional problems only the surface of the domain needs to be discretized. This means that, compared to FEM domain type analysis, a boundary analysis results in a substantial reduction in data preparation. At the same time, and due to the inherent characteristics of its formulation, BEM provides very accurate results for problems containing strong geometrical discontinuities. This makes BEM a powerful numerical tool for modelling crack problems [2].

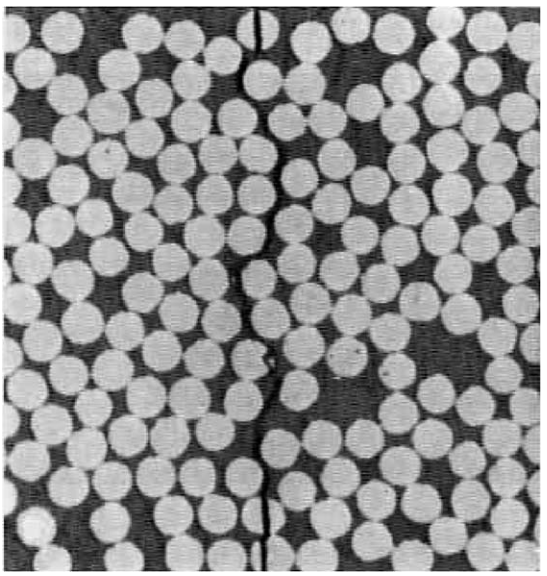

Fig. 1. Complete transverse crack in a unidirectional composite ply.

BEM has been extensively employed to analyse a variety of problems involving two-dimensional interface cracks. On the other hand, and according to the authors' knowledge, there are no reported results for three-dimensional problems. Among others, two-dimensional BEM analysis are reported by Cho et al. [3], who analysed the problem of interface cracks in dissimilar anisotropic materials; Yuuki and Xu [4], who evaluated the effect of residual stresses; Sladeck and Sladeck [5,6], who conducted studies on $T$-stresses and dissimilar elastoplastic materials; Kwon and Dutton [7], who tackled the problem of cracks in the direction normal to the bimaterial interface; and Selcuk et al. [8] and Beer [9], who used BEM for the prediction of interfacial crack propagation. Likewise, París et al. [10–13] studied the effect of crack-face contact on the fibre/matrix debonding, while Lui and Xu [14] considered the effect of the fibre coating on the debonding process.

Although many authors propose displacement and stress extrapolation methods to determine stress intensity factors from BEM results (see for example Tan and Gao [15], Yuuki and Cho [16], Mao and Sun [17] and He et al. [18]), $J$-integral methods constitute a more robust approach. Being an energy approach, $J$-integral methods eliminate the need to solve local crack tip fields accurately, since if integration domains are defined over a relatively large portion of the mesh, accurate modelling of the crack tip is unnecessary, because the contribution to $J$-integral of the crack tip fields is not significant. At the same time, BEM is specially suited for the evaluation of path independent integrals, since the required stresses, strains and derivatives of displacements at internal points can be directly obtained from their boundary integral representations. It also has been shown that BEM produces more accurate stresses and strains at internal points when compared with other numerical techniques, and therefore better results can be achieved. Application of the $J$-integral methodology for two-dimensional interface cracks can be found in the works by Miyazaki et al. [19] and de Paula and Aliabadi [20].

Among the available schemes for the numerical computation of the $J$-integral in three dimensions, the Energy Domain Integral (EDI) due to Moran and Shih [21] is employed in this work. Previous work by one of the authors has proved the versatility and efficiency of the EDI in the three-dimensional BEM analysis of isotropic cracked bodies [22,23]. Together with the EDI the interaction or $M_1$-integral methodology due to Chen and Shield [24] is employed in this work for decoupling the $J$-integral into the mixed-mode stress intensity factors. The $M_1$-integral methodology is based on the superposition of two equilibrium states, given by the

actual problem and a set of auxiliary known solutions. This approach has been recently reported in a number of papers using FEM to compute stress intensity factors along three-dimensional interface cracks (see Gosz et al. [25], Nagashima, Omoto and Tani [26], and Im et al. [27]). Using BEM the $M_1$-integral methodology has been implemented for two-dimensional cracks by Miyazaki et al. [19].

## 2. *J*-integral and stress intensity factor computation

### 2.1. The energy domain integral

Consider a three-dimensional crack front with a continuously turning tangent as depicted in Fig. 2(a). Define a local coordinate system $x^*$ at position $\eta$, where the crack energy release rate is evaluated, given by $x_1^*$ normal to the crack front, $x_2^*$ normal to the crack plane, and $x_3^*$ tangent to the crack front.

Following Natha and Moran [28], the energy release rate $G(\eta)$ due to crack extension in its own plane along a three-dimensional crack front takes the form (see Fig. 2)

$$G(\eta) = \lim_{C\to 0} \xi_k(\eta) \int_{C(\eta)} (w \cdot \delta_{ki} - \sigma_{ij}^* u_{j,k}^*) n_i \, \mathrm{d}C, \tag{1}$$

where $w$ is the strain energy density, $\sigma_{ij}^*$ and $u_{j,k}^*$ are Cartesian components of stress and displacement derivatives expressed in the local system $x^*$, $\xi_k(\eta)$ is the unit outward normal to the crack front in the local crack plane $x_1^*$–$x_3^*$, $n_i$ is the unit vector normal to the contour $C(\eta)$ (which lies in the $x_1^*$–$x_2^*$ plane), and $\mathrm{d}C$ is the differential of the arc length $C$. It is worth noting that, although Eq. (1) comes from a two-dimensional analysis, it applies for the three-dimensional case, as in the limit as $C \to 0$, plain strain conditions prevail so that three-dimensional fields approach to the plane problem.

In order to derive the equivalent domain representation of Eq. (1), we consider a small segment $L_c$ of the crack front that lies in the local $x_1^* - x_3^*$ plane as shown in Fig. 2(b). Next we assume that the segment undergoes a virtual crack advance in the plane of the crack, and we define the magnitude of the advance at each point $\eta$ as $\Delta a(\eta)$. We note that $\Delta a(\eta)$ varies continuously along $L_c$ and vanishes at each end of the segment. Now let

$$\overline{G}(\eta) = \int_{L_c} G(\eta) \Delta a(\eta) \, \mathrm{d}\eta, \tag{2}$$

where $G(\eta)$ is the integral defined in Eq. (1). When $G(\eta)$ belongs to the point-wise energy release rate, $\overline{G}$ gives the total energy released when the finite segment $L_c$ undergoes the virtual crack advance.

The appropriate domain form of the point-wise crack-tip contour integral can be obtained from Eq. (2) by considering a tubular domain $V$ surrounding the crack segment (see Fig. 3). As shown in the figure, the surface $S_t$ is formed by translating the contour $C$ along the segment $L_c$, and $S_o$ stands for the outer surface of $V$ including the ends. Next an auxiliary function $q$ is introduced, which is sufficiently smooth in $V$ and it is defined on the surfaces of $V$ as follows:

$$q_k = \begin{cases} \Delta a(\eta) \cdot \xi_k(\eta), & \text{on } S_t, \\ 0, & \text{on } S_o. \end{cases} \tag{3}$$

Finally, in the limit as the tubular surface $S_t$ is shrunk onto the crack segment $L_c$ and in the absence of crack face tractions, we obtain the domain integral:

$$\overline{G} = \int_V (\sigma_{ij}^* u_{j,k}^* - w \cdot \delta_{ki}) q_{k,i} \, \mathrm{d}V. \tag{4}$$

In absence of body forces the integral $\overline{G}$ given in Eq. (4) reduces to the domain representation of the familiar *J*-integral. If it is assumed that $G(\eta)$ is constant along $L_c$, it follows directly from Eq. (2) that:

$$J(\eta) = G(\eta) = \frac{\overline{G}}{\int_{L_c} \Delta a(\eta) \, \mathrm{d}\eta}. \tag{5}$$

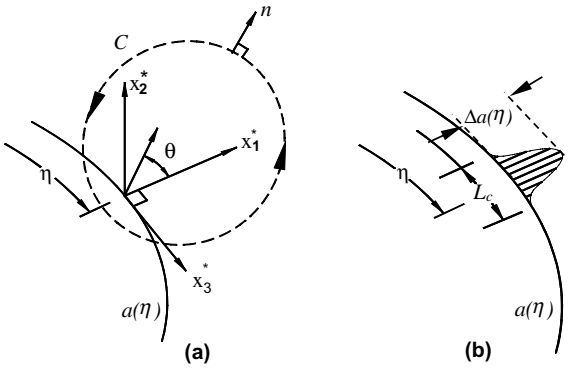


Fig. 2. (a) Definition of the local orthogonal Cartesian coordinates at point $\eta$ on the crack front and (b) virtual crack front advance.

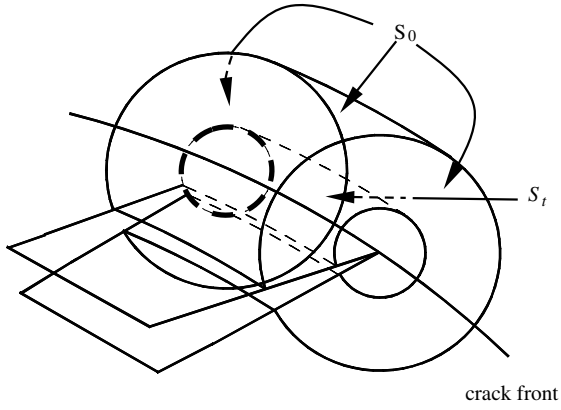


Fig. 3. Tubular domain surrounding a segment of the crack front.

### 2.2. The interaction integral

In this section, the interaction or $M_1$-integral methodology for decoupling three-dimensional mixed-mode stress intensity factors in bimaterial interface cracks is presented. In order to make sure the meaningfulness of the stress intensity factors we must consider the linear elastic solution of the *open model* of interface cracks. It is assumed in this model that the small contact zone that always develops at the crack tip is physically non-relevant (see Section 5 for further details). We label the material occupying the upper half-plane as material 1 with Young modulus $E_1$ and Poisson ratio $\nu_1$ (see Fig. 4). The material occupying the lower half-plane has Young modulus $E_2$ and Poisson ratio $\nu_2$. Let us consider now two equilibrium states with field variables denoted by the superscripts (1) and (2), respectively. Superposition of the two equilibrium states leads to another one, (1 + 2). Then the stress intensity factors $K_j^{(1+2)}$ can be written as

$$K_j^{(1+2)} = K_j^{(1)} + K_j^{(2)} \quad (j = \mathrm{I}, \mathrm{II}, \mathrm{III}). \tag{6}$$

The relationship between the $J$-integral and the stress intensity factors of an interface crack [29] is

$$J = \frac{1}{E^* \cosh^2(\pi\varepsilon)} \left[K_{\mathrm{I}}^2 + K_{\mathrm{II}}^2\right] + \frac{1}{2\mu^*} K_{\mathrm{III}}^2, \tag{7}$$

where $E^*$ and $\mu^*$ are the effective Young and shear modulus,

$$\frac{1}{E^*} = \frac{1}{2}\left(\frac{1-\nu_1^2}{E_1} + \frac{1-\nu_2^2}{E_2}\right), \quad \frac{1}{\mu^*} = \frac{1}{2}\left(\frac{1}{\mu_1} + \frac{1}{\mu_2}\right) \tag{8}$$

and $\varepsilon$ stands for the bimaterial constant:

$$\varepsilon = \frac{1}{2\pi} \ln\left[\frac{\kappa_1\mu_2 + \mu_1}{\kappa_2\mu_1 + \mu_2}\right]. \tag{9}$$

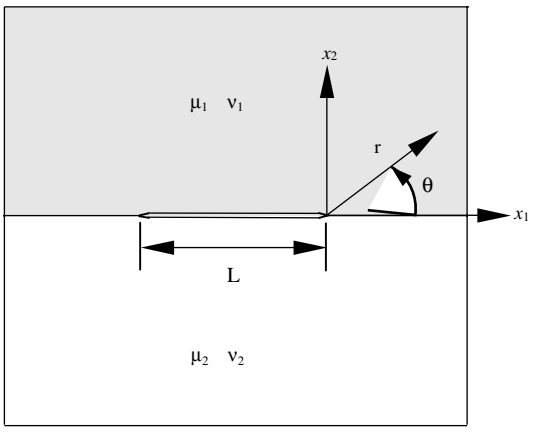


Fig. 4. Schematic representation of bimaterial plate with an interface crack.

Using the above relationships, the stress intensity factors can be related to the $J$-integral for the superimposed state (1 + 2) resulting in

$$J^{(1+2)} = \frac{1}{E^* \cosh^2(\pi\varepsilon)} \left[\left(K_{\mathrm{I}}^{(1+2)}\right)^2 + \left(K_{\mathrm{II}}^{(1+2)}\right)^2\right] + \frac{1}{2\mu^*}\left(K_{\mathrm{III}}^{(1+2)}\right)^2. \tag{10}$$

Eq. (10) can be rewritten in terms of the stress intensity factors for the equilibrium states (1) and (2), to give:

$$J^{(1+2)} = J^{(1)} + J^{(2)} + \frac{2}{E^* \cosh^2(\pi\varepsilon)} \left[K_{\mathrm{I}}^{(1)} K_{\mathrm{I}}^{(2)} + K_{\mathrm{II}}^{(1)} K_{\mathrm{I}}^{(2)}\right] + \frac{1}{\mu^*} K_{\mathrm{III}}^{(1)} K_{\mathrm{III}}^{(2)}. \tag{11}$$

Then, the $M_1$-integral is defined as

$$M_1 = J^{(1+2)} - J^{(1)} - J^{(2)} = \frac{2}{E^* \cosh^2(\pi\varepsilon)} \left[K_{\mathrm{I}}^{(1)} K_{\mathrm{I}}^{(2)} + K_{\mathrm{II}}^{(1)} K_{\mathrm{I}}^{(2)}\right] + \frac{1}{\mu^*} K_{\mathrm{III}}^{(1)} K_{\mathrm{III}}^{(2)}. \tag{12}$$

Using Eq. (4) a domain representation of the $M_1$-integral can be obtained as follows:

$$M_1 = \int_V \left(\sigma_{ij}^{*(1)} u_{j,k}^{*(2)} + \sigma_{ij}^{*(2)} u_{j,k}^{*(1)} - \sigma_{ij}^{*(1)} \varepsilon_{ij}^{*(2)} \delta_{ki}\right) q_{k,i} \, \mathrm{d}V. \tag{13}$$

For the decoupling of the mixed-mode stress intensity factors, the problem under consideration is selected as equilibrium state (1), so that the field variables $\sigma_{ij}^{*(1)}$ and $u_{j,k}^{*(1)}$ will be obtained in this work from the results of a boundary element analysis. On the other hand, the plain-strain solutions for the asymptotic crack-tip fields with prescribed stress intensity factors $K_{\mathrm{I}}$, $K_{\mathrm{II}}$ and $K_{\mathrm{III}}$, are selected as equilibrium state (2). Then the field variables related with the equilibrium state (2), $\sigma_{ij}^{*(2)}$, $u_{j,k}^{*(2)}$ and $\varepsilon_{ij}^{*(2)}$ are calculated from these asymptotic solutions. Finally the $M_1$-integral defined in Eq. (13) can be calculated, using the field variables related with the equilibrium states (1) and (2). By using three sets of asymptotic solutions, $(K_{\mathrm{I}}^{(2)} = 1, K_{\mathrm{II}}^{(2)} = 0, K_{\mathrm{III}}^{(2)} = 0)$, $(K_{\mathrm{I}}^{(2)} = 0, K_{\mathrm{II}}^{(2)} = 1, K_{\mathrm{III}}^{(2)} = 0)$ and $(K_{\mathrm{I}}^{(2)} = 0, K_{\mathrm{II}}^{(2)} = 0, K_{\mathrm{III}}^{(2)} = 1)$, it is possible to obtain the stress intensity factor solutions for individual modes from Eq. (12) as follows:

$$\begin{aligned} K_{\mathrm{I}}^{(1)} &= \frac{E^* \cosh^2(\pi\varepsilon)}{2} M_1^a, \\ K_{\mathrm{II}}^{(1)} &= \frac{E^* \cosh^2(\pi\varepsilon)}{2} M_1^b, \\ K_{\mathrm{III}}^{(1)} &= \frac{E^* \cosh^2(\pi\varepsilon)}{2} M_1^c, \end{aligned} \tag{14}$$

where $M_1^a$, $M_1^b$ and $M_1^c$ are the values of the $M_1$-integral calculated using the three sets of asymptotic solutions. Expressions of the above referred asymptotic solutions are given in Appendix A.

It is important to point out that the present implementation of the $M_1$-integral approach is only valid for straight crack fronts. For the application of the $M_1$-integral along curved crack fronts extra terms need to be included in Eq. (13), [25]. At the same time it is worth to note that because the $M_1$-integral is based upon the assumption that the near-crack tip fields is asymptotic to the plain strain field, it is not strictly applicable at the intersection of the crack front with a free surface. It turns out that at the intersection of the crack front and the free surface, the singularity in the stress field is more severe than the usual $1/\sqrt{r}$ singularity [30].

## 3. Computation of displacement derivatives, stresses and strains

In order to account for the non-homogeneous material properties, a subdomain BEM formulation is used in this work. The modelling strategy is illustrated in the schematic representation in Fig. 5, for a model with two subdomains, $\Omega_{\mathrm{I}}(X)$ and $\Omega_{\mathrm{II}}(X)$, with external boundaries $\Gamma_{\mathrm{I}}(x)$ and $\Gamma_{\mathrm{II}}(x)$ respectively. Both subdomains share an interface boundary $\Gamma_{12}(x)$, a portion of which is debonded and thus an interface crack is introduced. Following the standard procedure in BEM, the displacement boundary integral equation relating the boundary displacements $u(x)$ with the boundary traction $t(x)$ is applied to each of the subdomains, and the equilibrium, $t_2^{\mathrm{I}} = -t_2^{\mathrm{II}}$, and continuity, $u_2^{\mathrm{I}} = u_2^{\mathrm{II}}$, conditions enforced at the common interface $\Gamma_{12}(x)$. It is worth noting that the implemented BEM code is not capable to detect contact between the crack surfaces, and so, its application is restricted to open cracks. For further details on the subdomain BEM formulation the reader is referred to the book by Brebbia et al. [31].

The computation of the EDI and $M_1$-integral are included in the BEM code as a post-processing procedure,

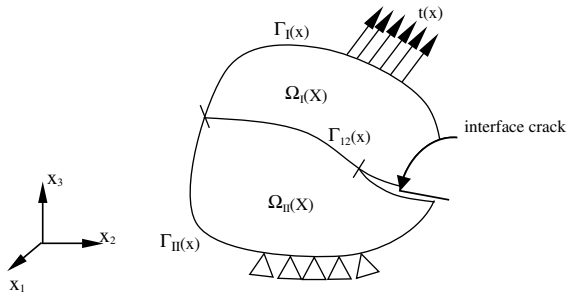


Fig. 5. Schematic representation of the multidomain technique for a non-homogeneous body.

and so it could be applied to the results from a particular model at a later stage. The required stresses, strains and derivatives of displacements at internal points are directly obtained from their boundary integral representations, while for boundary points they are evaluated from the boundary displacements and tractions.

### 3.1. Internal points

As has been stated in Section 2, the computation of the $J$-integral and the application of the $M_1$-integral methodology requires the stress and displacement derivative fields $\sigma_{ij}^*$ and $u_{j,k}^*$ to be known within the integration volume $V$. Although these quantities must be expressed in the local crack-front coordinate system $x^*$, in this work, and for the sake of simplicity, they will be firstly computed in the global system $x$ and later transformed to the local system $x^*$. Bearing this in mind, and in order to integrate the computation of the fracture parameters into the BEM formulation, derivatives of the displacements at internal points $X'$ are obtained from their boundary integral representations [31]:

$$u_{i,m}(X') = \int_\Gamma U_{ij,m}^* t_j \,\mathrm{d}\Gamma - \int_\Gamma T_{ij,m}^* u_j \,\mathrm{d}\Gamma, \tag{15}$$

where the terms $U_{ij,m}^*$ and $T_{ij,m}^*$ are the derivatives of the fundamental displacement $U_{ij}^*$, and traction $T_{ij}^*$ solution, and the boundary $\Gamma$ corresponds to that of the zone where the point $X'$ lies on.

Once the displacement derivatives $u_{i,m}$ are known, stresses $\sigma_{ij}$ and strains $\varepsilon_{ij}$ can be computed using the basic continuum mechanics relationships:

$$\varepsilon_{ij} = \frac{1}{2}(u_{i,j} + u_{j,i}), \tag{16}$$

$$\sigma_{ij} = 2\mu\varepsilon_{ij} + \frac{2\mu v}{1-2v}\varepsilon_{kk}\delta_{ij}. \tag{17}$$

### 3.2. Boundary points

Displacement partial derivatives $u_{i,m}$ at boundary nodes could be obtained from Eq. (15), by taking the limit as point $X'$ moves to the boundary, i.e. $X' \to x'$. However, this procedure is computationally expensive because of the occurrence of hypersingular integrands [31]. To avoid this difficulty, stresses and strains, as well as the displacements on the model surface are evaluated in this work from the boundary displacements and tractions. Consider with this purpose a local cartesian system, $(x_1^0, x_2^0, x_3^0)$ such that $x_3^0$ is the unit vector in the normal direction to the boundary element (see Fig. 6). If $u_j^0$, $\varepsilon_{ij}^0$, $\sigma_{ij}^0$ and $t_j^0$ are the displacements, strains, stresses and tractions in the local system, stress components in the normal direction can be written as

$$\sigma_{i3}^0 = t_i^0, \quad i = 1,2,3. \tag{18}$$

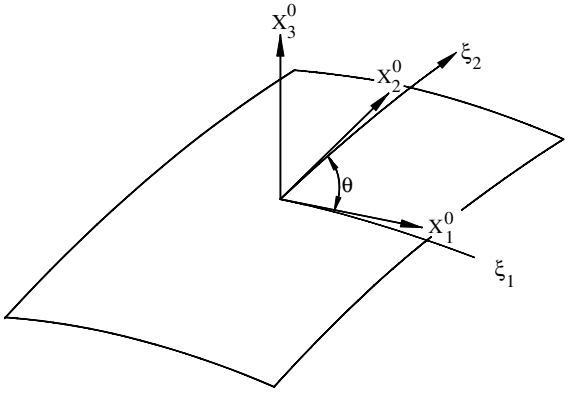


Fig. 6. Local Cartesian system for boundary stress calculation.

The remaining stress tensor components, $\sigma^0_{11}$, $\sigma^0_{12}$ and $\sigma^0_{22}$ can be expressed in terms of $t^0_3$ and the tangential strain tensor components $\varepsilon^0_{11}$, $\varepsilon^0_{12}$ and $\varepsilon^0_{22}$, by eliminating $\varepsilon^0_{33}$ from the general expression of Hooke's law. Thus

$$\sigma^0_{11} = \frac{1}{1-\nu}[\nu t^0_3 + 2\mu(\varepsilon^0_{11} + \nu\varepsilon^0_{22})], \tag{19a}$$

$$\sigma^0_{22} = \frac{1}{1-\nu}[\nu t^0_3 + 2\mu(\varepsilon^0_{22} + \nu\varepsilon^0_{11})], \tag{19b}$$

$$\sigma^0_{12} = 2\mu\varepsilon^0_{12}. \tag{19c}$$

Strain components $\varepsilon^0_{ij}$ can be found using Eq. (16), now applied in the local coordinate system. It is worth nothing that displacement derivatives in Eq. (16) are initially evaluated in the intrinsic element directions $(\xi_1, \xi_2)$ and then converted to the local coordinate system $x^0$, since boundary displacements are given in terms of the piecewise parametric representation (shape functions) of intrinsic coordinates.

Finally, the nine components of the partial displacement derivatives $u^*_{j,m}$ are computed. Using chain differentiation, derivatives of the displacements in the global system $u_{j,m}$, are related to the derivatives of the displacements with respect to the intrinsic boundary element directions $\partial u_i/\partial\xi_j$ as follows:

$$\frac{\partial u_i}{\partial \xi_j} = \frac{\partial u_i}{\partial x_k}\frac{\partial x_k}{\partial \xi_j}, \tag{20}$$

where $\partial x_k/\partial\xi_j$ is the Jacobian matrix of the transformation.

It can be seen that Eq. (20), once expanded, yields a set of six equations with the nine derivatives $u_{i,k}$ as unknowns. Three of these unknowns $u_{1,1}$, $u_{2,2}$ and $u_{3,3}$, can be directly calculated from the strain tensor components $\varepsilon_{11}$, $\varepsilon_{22}$ and $\varepsilon_{33}$, respectively by using Eq. (16). This leaves the system with six unknowns, which can be further reduced to three if the values of $\varepsilon_{11}$, $\varepsilon_{12}$ and $\varepsilon_{13}$ are substituted in Eq. (20) and then replaced in the system of equations. Finally, the three remaining unknowns are calculated using a set of three equations taken from the system generated by Eq. (20). It is worth noting that, since one or more of the derivatives $\partial u_k/\partial\xi_j$ can become simultaneously zero depending on the element orientation and shape, the selection of the three equations cannot be arbitrary, being then necessary to make a special selection in each case.

## 4. Boundary element implementation

As has been stated in Section 2, expressions (4) and (13) allow the computation of $J$-integral and the mixed-mode stress intensity factors at any position $\eta$ on the crack front to be carried out. In each case, this requires the evaluation of a volume integral within closed domains that enclose a segment of the crack front $L_c$. A natural choice here is to make $\eta$ coincident with the element nodes on the crack front, while $L_c$ is taken as the element or element sides at which points $\eta$ lies (see Fig. 7). The portion of the model domain in which the volume integrals are evaluated is discretized using 27-noded isoparametric (brick) cells, over which stresses, strains and displacements derivatives are approximated by products of the cell interpolation functions $\Psi_i$ and the nodal values of $\sigma_{ij}$, $\varepsilon_{ij}$ and $u_{i,j}$. Nodal values of this variable are computed following the procedures introduced in Section 3, depending on whether the node is internal or lies on the model boundary. Volume discretization is designed to have a web-style geometry around the crack front, while the integration volumes are taken to coincide with the different rings of cells. This is illustrated in Fig. 8, where the frontal face of the model has been partially removed to show the crack and the integration domains.

As depicted in Fig. 7, three different cases need to be considered, depending on whether the node of interest $M$ is in the middle of an element side (mid-side node),

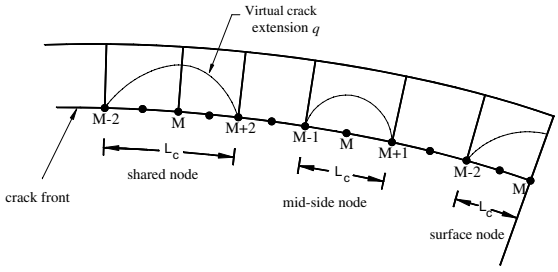


Fig. 7. Schematic representation of the volume cells in the crack front region illustrating the virtual crack extensions for a shared node, a mid-side node and a surface node.

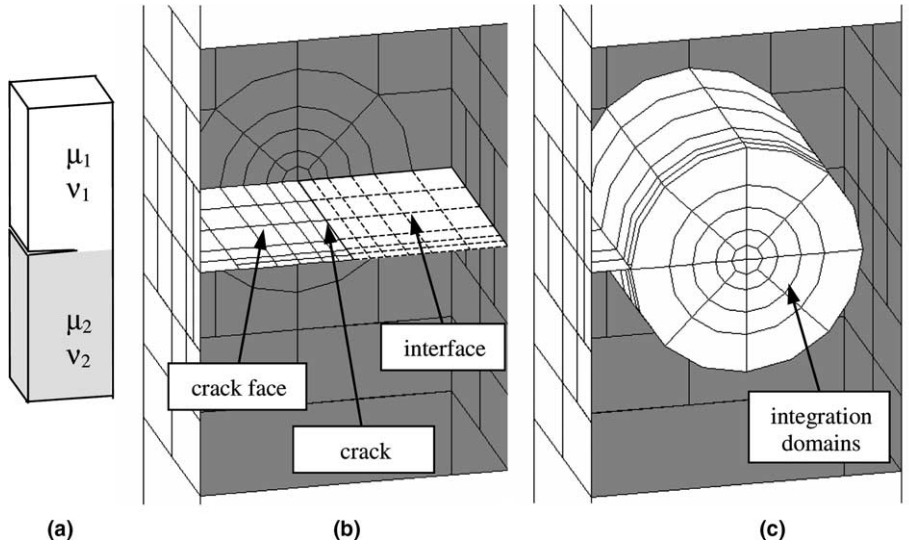


Fig. 8. (a) Problem geometry, (b) boundary element discretization and (c) integration domains.

it is shared by two elements (shared node), or it is located coincident with the external surface (surface node). If the node $M$ is a mid-side node or surface node, $L_c$ (the segment of the crack front over which the $M_1$-integral is computed) spans over one element, connecting nodes $M-1$, $M$, and $M+1$ and nodes $M-2$, $M-1$ and $M$, respectively. On the other hand, if $M$ is a shared node, $L_c$ spans over two elements, connecting nodes from $M-2$ to $M+2$.

In this work $q$ is defined to vary quadratically in the directions tangential and normal to the crack front. This bi-quadratic definition of $q$ has been employed with excellent results in the computation of EDI for cracks in homogeneous materials in previous works by one of the authors [22,23]. Within this approach, and considering that the evaluation point $\eta$ is at the middle of the crack front segment $L_c$, and $r_0$ is the radius of the integration domain, the function $q$ is written as

$$q(x^*) = \left|1 - \left(\frac{x_3^*}{L_c/2}\right)^2\right| \cdot \left[1 - \left(\frac{r}{r_0}\right)^2\right], \tag{21}$$

where $r$ is the distance from the crack front in the $x_1^* - x_2^*$ plane as depicted in Fig. 2.

Function $q$ is specified at all nodes within the integration volumes. Consistent with the isoparametric formulation, these $q$-values are given by

$$q = \sum_{i=1}^{27} \Psi_i Q^i, \tag{22}$$

where $\Psi_i$ are the shape functions defined within each volume cell and $Q^i$ are the nodal values for the $i$ th node. From the definition of $q$ (see Eq. (3)), $Q^i = 0$ if the $i$th node is on $S_o$, while for nodes inside $V$, $Q^i$ are given by interpolating between the nodal values on $L_c$ and $S_o$. Following standard manipulations:

$$q_{,j} = \sum_{i=1}^{27} \sum_{k=1}^{3} \frac{\partial \Psi_i}{\partial \zeta_k} \frac{\partial \zeta_k}{\partial x_j} Q^i, \tag{23}$$

where $\zeta_k$ are the coordinates in the cell isoparametric space and $\partial x_k/\partial \xi_j$ is the Jacobian matrix of the transformation given by

$$\overline{G} = \sum_{\text{cells in } V} \sum_{p=1}^{m} \left\{ \left(\sigma_{ij}^* u_{j,k}^* - \sigma_{ij}^* \varepsilon_{ij}^* \delta_{ki}\right) q_{k,i} \det\left(\frac{\partial x_j}{\partial \zeta_k}\right) \right\}_p w_p \tag{24}$$

and

$$M_1 = \sum_{\text{cells in } V} \sum_{p=1}^{m} \left\{ \left(\sigma_{ij}^{*(1)} u_{j,k}^{*(2)} + \sigma_{ij}^{*(2)} u_{j,k}^{*(1)} - \sigma_{ij}^{*(1)} \varepsilon_{ij}^{*(2)} \delta_{ki}\right) \times q_{k,i} \det\left(\frac{\partial x_j}{\partial \zeta_k}\right) \right\}_p w_p \tag{25}$$

respectively, where $m$ is the number of Gaussian points per cell, and $w_p$ are the weighting factors.

## 5. Analysis of a fibre/matrix interface crack under transverse loading

Oscillatory behaviour is an inherent feature of a linear elastic solution of the open model of interface cracks for non-vanishing bimaterial mismatch constant

$\varepsilon$ [32]. Stresses and displacements start to oscillate when the crack tip is approached. A consequence of these oscillations is that the solution predicts an interpenetration of the crack faces. As was shown by Comninou [33], this oscillatory behaviour of the open model solution is avoided assuming a contact zone adjacent to the crack tip in the so-called *contact model* of interface cracks. However, it is not unusual in engineering practice for the region of these oscillations to be physically non-relevant, it frequently being of atomic of subatomic size. The concept of small-scale contact introduced by Rice [34] to characterize such a situation, provides a theoretical base for the meaningfulness of the stress intensity factors when applied to interface cracks.

A fibre/matrix interface crack is a particular case of interface crack. High-resolution numerical BEM models [10,11] and exact analytical solutions [35] have shown that for arc-shaped debonds an extensive region with negative opening (overlapping) before oscillation of the solution may, depending on the debonding length, arise. The problem must be under these circumstances modelled in accordance with Comninou conclusions [33] as appears in Fig. 9 [10,11]. Region I represents perfect bonding between fibre and matrix whereas Regions II and III represents the debonded part, Region II corresponding to the contact zone and Region III corresponding to the opened part of the debonded zone. A physical explanation of the relative sizes of overlapping predicted by the analytical solutions and the BEM models is given in [10]. It can be noticed that when the debonding starts to reach approximately 60° a contact zone of physical meaning can be detected [10].

In what follows the numerical tool devised in the previous sections is employed in order to take into account

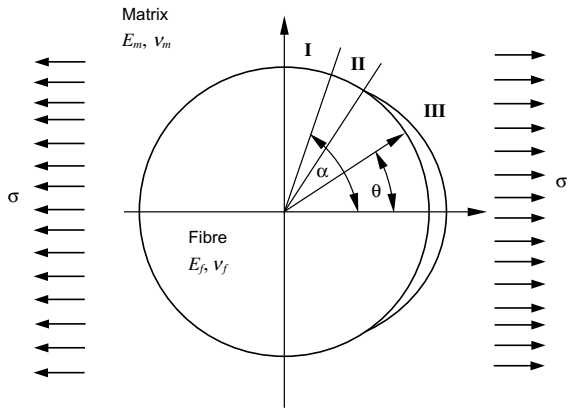


Fig. 9. Schematic representation of the cross-section of the fibre embedded in matrix and loaded transverse to the fibre axis. The fibre/matrix interface is partially debonded and three regions at the interface can be distinguished: I, perfect bonding; II, debonded zone with debond face contact; III, open zone (Ref. [10,11]).

the three-dimensional character of the problem without considering contact because this capabilities were not incorporated in the algorithm. This three dimensional model will in any case allow in the future the possibility of the interaction between longitudinal and circumferential growth of the crack to be studied.

### 5.1. Boundary element model

Fig. 10 illustrates the strategy proposed for the idealization of the BEM model. Fig. 10(a) corresponds to a micrograph in the direction transversal to the fibres in an unidirectional glass/epoxy laminate. It can be observed that although the fibres are distributed almost homogeneously, there are regions of the laminate that are rich in matrix. In order to limit the model size, it is assumed in this work that the fibres are packed in a periodic square array and that the damage takes place in one of the fibres by a pair of symmetric cracks running circumferentially between the fibre and the matrix (see Fig. 10(b)). At the same time the behaviour of the remaining portion of the laminate is idealized as transversely isotropic, with its isotropy plane perpendicular to the direction of the fibres (plane $xy$ in the figure).

The BEM model is composed by three regions with three planes of symmetry as depicted in Fig. 10(c). Regions I and II (isotropic) are used to model the representative volume element given by the fibre and the matrix around it, while Region III (transversely isotropic) models the effect of the remaining portion of the laminate and provides boundary conditions to the zone of interest. In order to introduce the transversely isotropic material behaviour, Region III was formulated using the correspondent fundamental solutions proposed by Loloi [36].

Model dimensions are given in Fig. 10(c) as a function of the radius of the fibre $R$, and in such way that the fibre volume fraction represents 60% of the representative volume element. Model thickness is $t = 1.5R$. The debond angle is selected $\alpha = 37°$ in order to avoid the occurrence of the crack face contact [10]. Elastic properties are $E_f = 7.08 \times 10^{10}$ MPa and $\nu_f = 0.22$ for the fibre, and $E_m = 2.79 \times 10^9$ MPa and $\nu_m = 0.33$ for the matrix. The bimaterial index for this material combination is $\varepsilon = 0.074$. The properties for the transversely isotropic material are $E_x = 8.9 \times 10^9$ MPa and $\nu_{xy} = 0.27$, and $E_z = 43 \times 10^9$ MPa and $\nu_{xz} = 0.06$ for the isotropy plane and the direction of the fibres respectively (see coordinate system in Fig. 11). The discretized model geometry is illustrated in Fig. 11. It consists of 291 elements and 1353 nodes. Forty-nine elements are used for the crack face discretization. Four rings of cells with radii $r/a$ = 0.18, 0.28, 0.39 and 0.46 are employed for $J$-integral and stress intensity factor computations. The number of cells used with this purpose is 252. Symmetry conditions were handled implicitly in the BEM formulation,

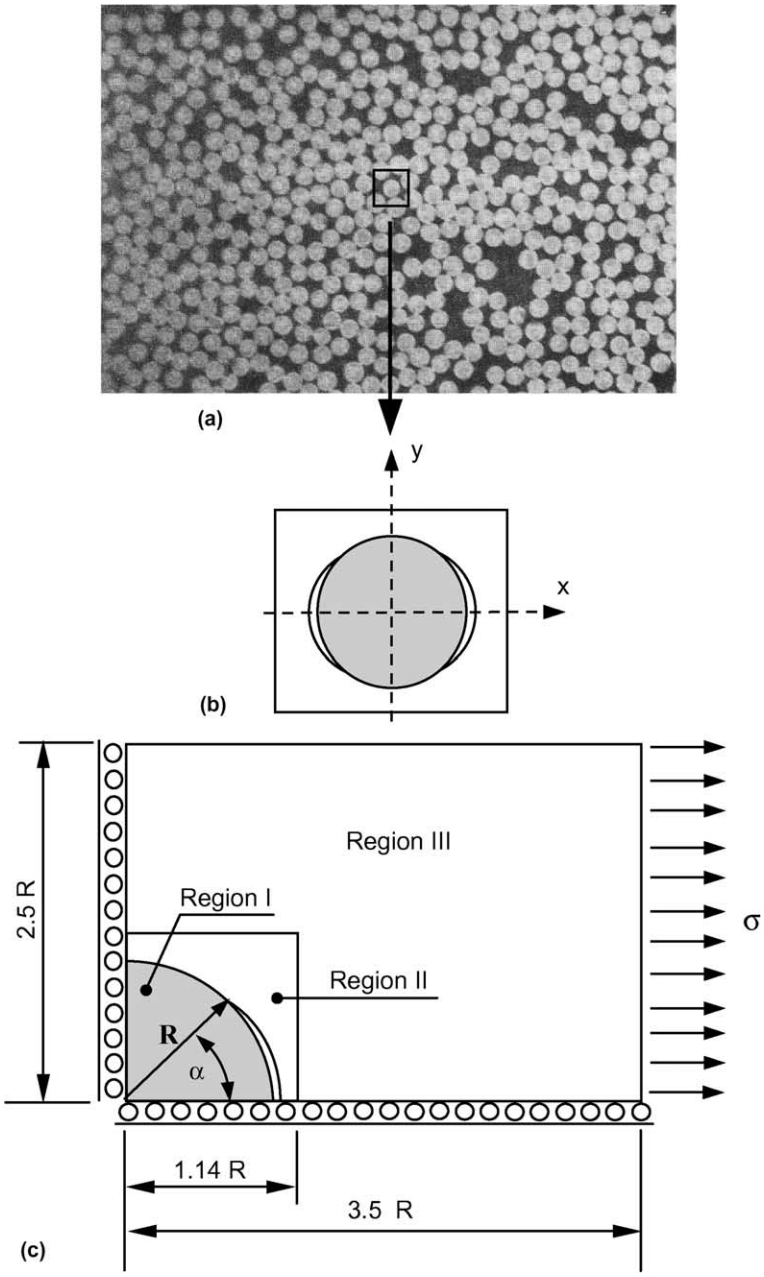


Fig. 10. 2D schematic representation of the 3D BEM model: (a) micrograph in the direction transversal to the fibres in unidirectional glass/epoxy laminate, (b) square cell with symmetric debond cracks, (c) model dimensions and boundary conditions.

in such a way that symmetry planes do not need to be discretized (see Fig. 11). This procedure redounds in both computer memory savings and numerical efficiency for the BEM implementation. Due to space restrictions the details of the implementation are not been presented in this work. For a comprehensive description of the procedure the reader is referred to the work by Paris and Garrido [37].

The model is analysed considering five different material combinations. The first case is devised for validation purposes and to allow comparison with two-dimensional results. With this idea all the three regions of the model are considered isotropic and with the elastic properties of the fibre (note that this assumption reduces the problem to that of a circular arc crack in a homogeneous panel). At the same time the displacements in the direc-

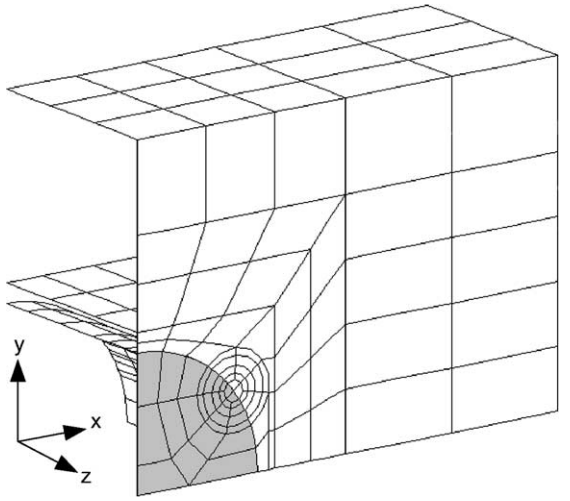


Fig. 11. Boundary element model for the fibre/matrix interface crack.

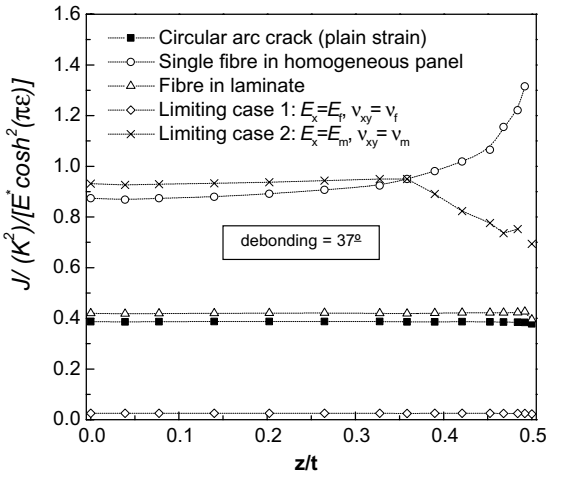


Fig. 12. *J*-integral along the crack front for the fibre/matrix interface crack.

tion of the thickness are restricted in order to obtain plain strain conditions. The other four cases are devoted to study the influence of the material properties of Region III on the fibre/matrix interface crack behaviour. Thus, in the second case the event of single fibre in a homogeneous panel is considered, and so the elastic properties for Region III are set identical to those of the matrix material (Region II). Cases three to five assume a transversely isotropic behaviour for Region III. In case three, elastic properties of Region III are those of the glass/epoxy laminate given in the previous paragraph, while cases four and five consider the two limiting cases for which the elastic properties of the isotropy plane coincide with those of the fibre ($E_x = E_f, v_{xy} = v_f$) and the matrix ($E_x = E_m, v_{xy} = v_m$) respectively.

### 5.2. Results and discussion

*J*-integral results obtained along the crack front for the five material combinations are plotted in Fig. 12. The origin of the normalized coordinate *z*/*t* corresponds to the specimen mid-plane, and all values are normalized with respect to the *J*-integral result for a 2D crack in an infinite bimaterial plate $J_o = (K)^2/[E^*\cosh^2(\pi\varepsilon)]$, where $K = \sigma^\infty[(1 + 4\varepsilon^2)\pi a]^{1/2}$ and $E^*$ is the effective elastic modulus for the fibre/matrix bimaterial combination. As is expected, the plain-strain homogeneous model results in a constant *J*-integral value along the complete crack front. On the other hand, the model of the single fibre presents the strongest 3D effect, with the most marked variation of the *J*-integral value along the crack front. Its largest value takes place at the free surface ($z/t = 0.5$). If the effect of the fibres in the laminate is considered (results labelled as "fibre in laminate" in Fig. 12), the large stiffness of the specimen in the direction of the thickness makes the crack to behave as in the plain strain model, and a constant *J*-integral value is obtained along the complete crack front. The two other sets of results correspond to the limiting cases for which the elastic properties of the isotropy plane are taken the same to those of the matrix and the fibre respectively. When the elastic properties are those of the matrix, the *J*-integral value is almost the same to that obtained for the single fibre example at the interior of the specimen, but it drops at the free surface. Finally, when the elastic properties of the isotropy plane are those of the fibre (the most rigid of all cases analysed) *J*-integral presents its lowest level, and similarly to the homogeneous case, it presents a constant value along the complete crack front.

The above results allow explaining experimental observations as those reported by Meurs [1], who tested a single glass-fibre-reinforced specimen in transverse loading. The vicinity of the upper and lower specimen surfaces are shown in Fig. 13 for four increasing load steps ($\sigma_1$ to $\sigma_4$). In each micrograph, the locations of the fibre ends are given by the dotted lines. Note that in accordance with the numerical results for the single fibre example; debond crack initiates at the specimen surface, where the maximum *J*-integral value is achieved. It is also worth to note that this analysis for single fibre can be assimilated to the situation in an actual laminate for which an irregular packing of fibres due to inhomogeneous fibre distribution leads to a zone rich in matrix.

Stress intensity factor results are presented for the three modes of cracking in Figs. 14–16. Results are normalized with respect to $\sigma^\infty\sqrt{\pi a}$. Fig. 14 allows observing that the behaviour of $K_I$ along the crack front is very

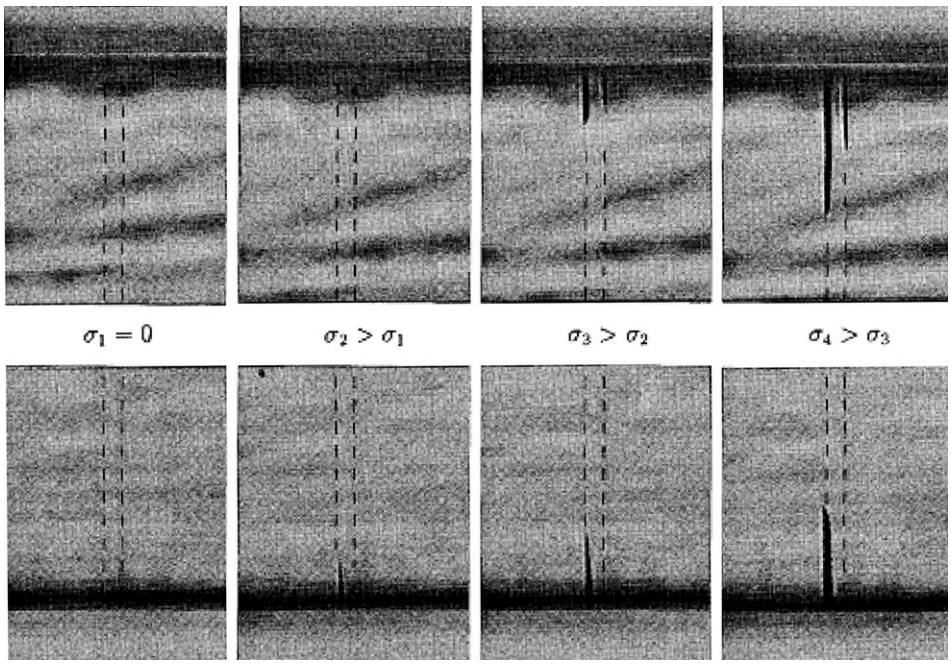


Fig. 13. Optical micrographs of initiation of debonding in a transverse test (from Ref. [1]).

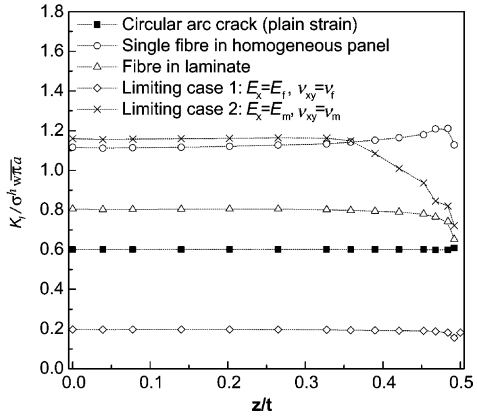


Fig. 14. $K_I$ along the crack front for the fibre/matrix interface crack.

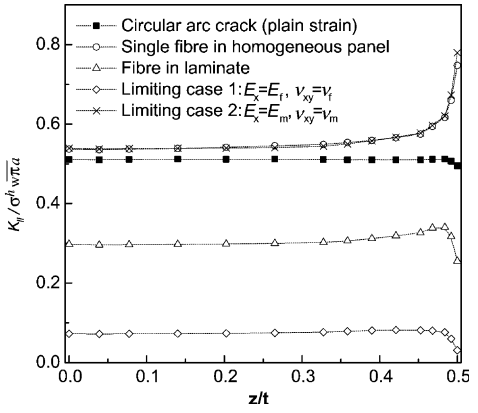


Fig. 15. $K_{II}$ along the crack front for the fibre/matrix interface crack.

similar to that exhibited by the $J$-integral, that is, the maximum $K_I$ values are obtained for the cases with the largest material mismatch between the fibre and the surrounding material. It is also worth to note that with the only exception of the limiting case for which the elastic properties of the isotropy plane are taken coincident with those of the matrix, $K_I$ results present a constant value along most of the crack front. Three-dimensional effects are very weak, and restricted only to a small portion of the crack front in the vicinity of the free surface. Results for $K_{II}$ (see Fig. 15), show a strong three-dimensional effect in the case of the single fibre, and when the elastic properties in the isotropy plane are those of the matrix. For these two cases, $K_{II}$ markedly increase in the vicinity of the free surface. Finally, $K_{III}$ results, increases towards the free surface for all material combinations, showing a marked dependence with the material properties (see Fig. 16).

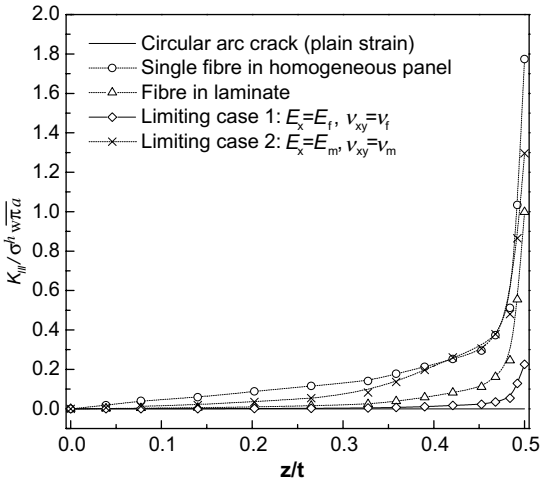


Fig. 16. $K_{III}$ along the crack front for the fibre/matrix interface crack.

## 6. Conclusions

In this paper, a boundary element methodology for the three-dimensional analysis of bimaterial interface cracks has been presented. The interface crack analysis is addressed using a multidomain BEM formulation in order to account for the different material properties at both sides of the crack. Fracture mechanics parameters, namely $J$-integral and stress intensity factors, are computed along the crack front using the Energy Domain Integral and the $M_1$-integral methodologies. These are implemented as a post-processing technique, and so it can be applied to the results from a particular model at a later stage. The implementation takes advantage of the efficiency of the boundary integral equation to directly obtain the required displacement derivatives, stress and strain fields from their boundary integral representations.

The devised numerical tool is employed to analyse the problem of a fibre/matrix interface crack under transverse loading in order to assess its three-dimensional character. This three dimensional model will in any case allow in the future the possibility of the interaction between longitudinal and circumferential growth of the crack to be studied. Obtained results show the key role played by the relative elastic properties of the fibre, the matrix and the laminate on the state of mixed mode fracture. The case of a single debonded fibre in a homogeneous panel constitutes the most severe condition, as it presents a large material mismatch with low lateral constraint. On the other hand, a fibre in a laminate behaves very similarly to a plain-strain case analysis, showing that three-dimensional effects are very weak for this case. Finally, the computed mixed-mode stress intensity factor show, that for most of the material combinations studied, $K_I$ does not present important variations along the crack front, including the region in the vicinity of the free lateral surface. In contrast, the boundary layer effect is marked for $K_{II}$ and $K_{III}$.

## Acknowledgments

This work was financed by grant PEI 6494 of the Consejo Nacional de Investigaciones Científicas y Técnicas de la República Argentina (CONICET) and the University of Mar del Plata. The authors wish to express their thanks to Prof. F. París and V. Mantič (University of Seville, Spain) for helpful discussion and kindly providing much of the reference material used in this work.

## Appendix A

In this appendix the auxiliary asymptotic solutions of stress $\sigma_{ij}$ and displacements $u_i$, for the extraction of the mode I and II stress intensity factors are given. The expressions are due to Williams [32], and they are referred to the in the local $x_1$–$x_2$ plane (see Fig. 4).

$$(\sigma_{11})_j = \frac{K_I}{2\sqrt{2\pi r}}\left[\omega_j f_{11}^{I} - \frac{1}{\omega_j}\cos(\theta-\overline{\Theta})\right] - \frac{K_{II}}{2\sqrt{2\pi r}}\left[\omega_j f_{11}^{II} + \frac{1}{\omega_j}\sin(\theta-\overline{\Theta})\right], \tag{A.1}$$

$$(\sigma_{22})_j = \frac{K_I}{2\sqrt{2\pi r}}\left[\omega_j f_{22}^{I} + \frac{1}{\omega_j}\cos(\theta-\overline{\Theta})\right] - \frac{K_{II}}{2\sqrt{2\pi r}}\left[\omega_j f_{22}^{II} - \frac{1}{\omega_j}\sin(\theta-\overline{\Theta})\right], \tag{A.2}$$

$$(\sigma_{12})_j = \frac{K_I}{2\sqrt{2\pi r}}\left[\omega_j f_{12}^{I} - \frac{1}{\omega_j}\sin(\theta-\overline{\Theta})\right] - \frac{K_{II}}{2\sqrt{2\pi r}}\left[\omega_j f_{12}^{II} - \frac{1}{\omega_j}\cos(\theta-\overline{\Theta})\right], \tag{A.3}$$

$$(u_1)_j = \frac{K_I\sqrt{2\pi r}}{4\pi\mu_j}\left[\kappa_j\omega_j h_{11} - \frac{1}{\omega_j}h_{12} + \omega_j h_{13}\right] + \frac{K_{II}\sqrt{2\pi r}}{4\pi\mu_j}\left[\kappa_j\omega_j h_{21} - \frac{1}{\omega_j}h_{22} + \omega_j h_{23}\right], \tag{A.4}$$

$$(u_2)_j = \frac{K_I\sqrt{2\pi r}}{4\pi\mu_j}\left[\kappa_j\omega_j h_{21} - \frac{1}{\omega_j}h_{22} - \omega_j h_{23}\right] + \frac{K_{II}\sqrt{2\pi r}}{4\pi\mu_j}\left[-\kappa_j\omega_j h_{11} + \frac{1}{\omega_j}h_{12} + \omega_j h_{13}\right], \tag{A.5}$$

where

$$\alpha = \frac{1}{2\pi}\ln\left[\left(\frac{\kappa_1}{\mu_1}+\frac{1}{\mu_2}\right)\Big/\left(\frac{\kappa_2}{\mu_2}+\frac{1}{\mu_1}\right)\right], \tag{A.6}$$

$$\overline{\Theta} = \alpha\ln\left(\frac{r}{2a}\right) + \frac{\theta}{2}, \tag{A.7}$$

$$\kappa_j = 3 - 4\nu_j, \tag{A.8}$$

$$\omega_1 = e^{-\alpha(\pi-\theta)}, \tag{A.9}$$

$$\omega_2 = e^{\alpha(\pi+\theta)}, \tag{A.10}$$

$$f_{11}^{\mathrm{I}} = 3\cos\overline{\Theta} + 2\alpha\sin\theta\cos(\theta+\overline{\Theta}) - \sin\theta\sin(\theta+\overline{\Theta}), \tag{A.11}$$

$$f_{11}^{\mathrm{II}} = 3\sin\overline{\Theta} + 2\alpha\sin\theta\sin(\theta+\overline{\Theta}) + \sin\theta\cos(\theta+\overline{\Theta}), \tag{A.12}$$

$$f_{22}^{\mathrm{I}} = \cos\overline{\Theta} - 2\alpha\sin\theta\cos(\theta+\overline{\Theta}) + \sin\theta\sin(\theta+\overline{\Theta}), \tag{A.13}$$

$$f_{22}^{\mathrm{II}} = \sin\overline{\Theta} - 2\alpha\sin\theta\sin(\theta+\overline{\Theta}) - \sin\theta\cos(\theta+\overline{\Theta}), \tag{A.14}$$

$$f_{12}^{\mathrm{I}} = \sin\overline{\Theta} + 2\alpha\sin\theta\sin(\theta+\overline{\Theta}) + \sin\theta\cos(\theta+\overline{\Theta}), \tag{A.15}$$

$$f_{12}^{\mathrm{II}} = -\cos\overline{\Theta} - 2\alpha\theta\cos(\theta+\overline{\Theta}) + \sin\theta\sin(\theta+\overline{\Theta}), \tag{A.16}$$

$$h_{11} = \frac{1}{1+4\alpha^2}[\cos(\theta-\overline{\Theta}) - 2\alpha\sin(\theta-\overline{\Theta})], \tag{A.17}$$

$$h_{12} = \frac{1}{1+4\alpha^2}[\cos\overline{\Theta} + 2\alpha\sin\overline{\Theta}], \tag{A.18}$$

$$h_{13} = \sin\theta\sin\overline{\Theta}, \tag{A.19}$$

$$h_{21} = \frac{1}{1+4\alpha^2}[\sin(\theta-\overline{\Theta}) + 2\alpha\cos(\theta-\overline{\Theta})], \tag{A.20}$$

$$h_{22} = \frac{1}{1+4\alpha^2}[-\sin\overline{\Theta} + 2\alpha\cos\overline{\Theta}], \tag{A.21}$$

$$h_{23} = \sin\theta\cos\overline{\Theta}. \tag{A.22}$$

The difference between the properties of an interface crack under anti-plane strain and a mode III crack in an homogeneous medium is quite modest, as the displacement and stress fields at each side of the interface are the same to the mode III of separated homogeneous bodies [38]. In this way

$$(\sigma_{13})_j = -\frac{K_{\mathrm{III}}}{\sqrt{2\pi r}}\sin\left(\frac{\theta}{2}\right), \tag{A.23}$$

$$(\sigma_{23})_j = \frac{K_{\mathrm{III}}}{\sqrt{2\pi r}}\cos\left(\frac{\theta}{2}\right), \tag{A.24}$$

$$(u_3)_j = 2\frac{1+\nu_j}{E_j}\sqrt{\frac{2r}{\pi}}K_{\mathrm{III}}\sin\left(\frac{\theta}{2}\right). \tag{A.25}$$

## References


[1] Meurs P. Characterization of Microphenomena in transversely loaded composite material. PhD Thesis. Technische Universiteit Eindhoven, 1998.

[2] Aliabadi MH. Boundary element formulations in fracture mechanics. Appl Mech Rev 1997;50:83–96.

[3] Cho SB, Lee KR, Coi YS, Yuuki R. Determination of stress intensity factors and boundary element analysis for interface cracks in dissimilar anisotropic materials. Eng Fract Mech 1992;43:603–14.

[4] Yuuki R, Xu J-Q. Boundary element analysis of dissimilar materials and interface crack. Comput Mech 1994;14:116–27.

[5] Sladek J, Sladek V. Evaluation of the *T*-stress for interface cracks by the boundary element method. Eng Fract Mech 1997;56(6):813–25.

[6] Sladek J, Sladek V. Boundary element analysis for an interface crack between dissimilar elastoplastic materials. Comput Mech 1995;16:396–405.

[7] Kwon YW, Dutton R. Boundary element analysis of cracks normal to bimaterial interfaces. Eng Fract Mech 1991;40:487–91.

[8] Selcuk S, Hurd DS, Crouch SL, Gerberich WW. Prediction of interfacial crack path: a direct boundary integral approach and experimental study. Int J Fract 1994;67:1–20.

[9] Beer G. An efficient numerical method for modeling initiation and propagation of cracks along material interfaces. Int J Num Meth Eng 1993:3579–94.

[10] París F, del Caño JC, Varna J. The fiber-matrix interface crack—A numerical analysis using boundary elements. Int J Fract 1996;82:11–29.

[11] Varna J, París F, del Caño JC. The effect of crack-face contact on fibre/matrix debonding in transverse tensile loading. Compos Sci Technol 1997;57:523–32.

[12] París F, Correa E, Cañas J. Micromechanical view of failure of the matrix in fibrous composite materials. Compos Sci Technol 2003;63(7):1041–52.

[13] París F, Correa E, Mantič V. Study of kinking in transversal interface between fibre and matrix. In: 10th European Conference on Composites Materials, Brugge, Belgium, 2002.

[14] Lui YJ, Xu N. Modeling of interface cracks in fiber-reinforced composites with the presence of interphases using the boundary element method. Mech Mater 2000;32:769–83.

[15] Tan CL, Gao YL. Treatment of bimaterial interface crack problems using the boundary element method. Eng Fract Mech 1990;36:919–32.

[16] Yuuki R, Cho SB. Efficient boundary element analysis of stress intensity factors for interface cracks in dissimilar materials. Eng Fract Mech 1989;34:179–88.

[17] Mao R, Sun G. A study of the interaction between matrix crack and matrix-fibre interface. Eng Fract Mech 1995;51(3):469–77.

[18] He WJ, Lin DS, Ding HJ. A boundary element for crack analysis at a bimaterial interface. Eng Fract Mech 1994;49(3):405–10.

[19] Miyazaki N, Ikeda T, Soda T, Munakata T. Stress intensity factor analysis of interface crack using boundary

element method–Application of contour-integral method. Eng Fract Mech 1993;45(5):599–610.
[20] de Paula FA, Aliabadi MH. Boundary element analysis of interface cracks in dissimilar orthotropic materials using path independent contour integral. In: Boundary elements XIX 19th International conference on the boundary element method. Southampton, UK: Computational Mechanics Publications; 1997.
[21] Moran B, Shih CF. A general treatment of crack tip contour integrals. Int J Fract 1987:295–310.
[22] Cisilino AP, Aliabadi MH, Otegui JL. Energy domain integral applied to solve center and double-edge crack problems in three-dimensions. Theor Appl Fract Mech 1998;29:181–94.
[23] Cisilino AP, Aliabadi MH. BEM implementation of the energy domain integral for the elastoplastic analysis of 3D fracture problems. Int J Fract 1999;96:229–45.
[24] Chen FHK, Shield RT. Conservation laws in elasticity of the *J*-integral type. J Appl Math Phys (ZAMP) 1977;28: 1–22.
[25] Gosz M, Dolbow J, Moran B. Domain integral formulation for stress intensity factor computation along curved three-dimensional interface cracks. Int J Solids Struct 1998;35(15):1763–83.
[26] Nagashima T, Omoto Y, Tani S. Stress intensity factor analysis of interface cracks using X-FEM. Int J Num Meth Eng 2003;56:1151–73.
[27] Im S, Kim H-G, Kim YJ, Mode decomposition of three-dimensional mixed-mode cracks via two-state integrals 38 (36–37) (2001) 6405–26.
[28] Natha R, Moran B. Domain integrals for axisymmetric interface crack problems. Int J Solids Struct 1993;30(15): 2027–40.
[29] Nakamura T. Three-dimensional stress fields of elastic interface cracks. ASME J Appl Mech 1991;58:939–46.
[30] Xie M, Chaudhuri RA. Three-dimensional stress singularity at a bimaterial interface crack front. Compos Struct 1998;40(2):137–47.
[31] Brebbia CA, Telles JLF, Wrobel LC. Boundary Element Techniques. Berlin: Springer Verlag; 1984.
[32] Williams ML. The stress around a fault of crack in dissimilar media. Bull Seismol Soc Am 1959;49:199–204.
[33] Comninou M. The interface crack. ASME J Appl Mech 1977;44:631–6.
[34] Rice JR. Elastic fracture mechanics concepts for interface cracks. J Appl Mech 1988;55:98–103.
[35] Toya MA. crack along the interface of a circular inclusion embedded in an infinite solid. J Mech Phys Solids 1975;22:325–48.
[36] Loloi M. Boundary integral equation solution of three-dimensional elastostatic problems in transversely isotropic solids using closed-form displacement fundamental solutions. Int J Num Meth Eng 2000;48:823–42.
[37] Paris F, Garrido JA. An incremental procedure on the use of discontinuous elements in two dimensional contact problems. In: Brebbia, editor. Boundary Element VII. Springer; 1985.
[38] Broberg KB. Cracks and Fracture. Cambridge: Academic Press; 1999.